CORNELL UNIVERSITY

Center for Radiophysics and Space Research

ITHACA, N. Y.

[redacted]

[redacted]

CENTER FOR RADIOPHYSICS AND SPACE RESEARCH
CORNELL UNIVERSITY
ITHACA, NEW YORK

January 1965

CRSR 187

REPORT OF

FIELD TEST FOR TIGRIS

to the

NATIONAL AERONAUTICS AND SPACE ADMINISTRATION

TIGRIS FIELD TEST REPORT

I. INTRODUCTION

The TIGRIS camera system which was tested in the laboratory in September was taken to Capillo Peak Observatory near Albuquerque, New Mexico, to be tested there in dark sky conditions in October.* The three nights of October 6, 7 and 8 were dark and clear and very well suited for the tests.

The camera system functioned and displayed the expected exceptionally high sensitivity. With an f 2.8 lens and a two second exposure the night airglow could clearly be seen with dark objects in the foreground sharply silhouetted against it. With a similar aperture the most sensitive photographic film available does not show this in many minutes exposure.

It was unfortunate that the image orthicon tube which had undergone laboratory tests failed and had to be replaced by another incompletely tested one. Some of the difficulties that were encountered many be specific to this tube and further laboratory tests will be needed to ascertain this.

The field tests were useful not only in demonstrating the remarkable sensitivity but also in showing a variety of

---

* The Capillo Peak Observatory is operated by the Department of Physics of the University of New Mexico in Albuquerque and the very adequate facilities were made available for the test by Prof. Victor Regener. His kind help is gratefully acknowledged.

undesirable effects connected with the observation of a star field containing a great range of brightness together with a diffuse low intensity field which in this case was the night airglow. For the purpose for which this system is intended it is clear that the sensitivity makes it much preferable to photography even if recovery rather than telemetering were possible. The high definition (500 line picture) seems essential in order to be able to discrimate sufficiently many stars individually and thus avoid having them contribute to the unresolved background. The undesirable effects seen included very severe "shading", that is a variation of output level as a function of position in the image, a difficulty with the d.c. clamping, and a change in output as a result of a change in camera orientation. Several other undesirable but not necessarily incapacitating effects were also noted.

The data in this report are chiefly in the form of photographs of monitor and oscilloscope screens recording the camera's response to a variety of light sources in the night sky. Little attempt is made at present at an explanation of the various phenomena. As many associated facts as were recorded are pointed out in each case so as to give an overall picture including the dependence of the performance on system parameters. Detailed explanations will be attempted later in close consultation with experts in image orthicon design.

The pictures are arranged at the end of the report in the order in which they were taken. Although this creates some inconvenience in comparing some of the effects, the integration time sequences would be interrupted by any other arrangement. Also the fact that some prints are discussed in several sections means that a compromise in arrangement has to be made in any case. Under each print the central or most important constellation or other feature is listed along with as many other parameters as were available. The voltage is the beam voltage, the number of seconds is the integration time used to make the picture, and the clock time is the time of day when the picture was made.

II. SENSITIVITY

A small region between BD coordinates (6^h 32^* to 7^h 32^* R.A.) (-1° to $+10^\circ$ Dec.) was studied very carefully in Figures 8, 13, 14. The number of stars detected in each of these pictures along with the highest magnitude detectable are listed in the following table. The magnitudes

Fig.	Int. Time	# Stars	Highest Magnitude
8	2 sec.	37	6
13	16 sec.	80	7
14	32 sec.	84	7

The magnitudes were taken from the Henry Draper catalog. The closest stars which were resolved by the system were about $1/4^{o}$ apart, unresolved star pairs or groups of stars being therefore counted as one. These prints were made with a relatively high contrast on the monitor. This explains to some degree why only one magnitude was gained in increasing the integration time by a factor of 16 while not filling up the space between the brighter stars with the smeared out light of higher magnitude stars and night airglow. This is shown by the fact that figure 17, which was only a 2 sec. integration, but made with a low contrast setting on the monitor reveals nearly as many stars in the Canis Minor region as does figure 14 which was a 32 second integration made with a high contrast setting on the monitor. Both 17 and 14 were made with a 92 volt beam voltage. (The beam voltage rather than the beam current was measured for convenience. A higher beam voltage results in a lower beam current. The uniformity of the beam voltage to current relationship from tube to tube must be checked since the current determines the discharge rate of the target.) However, it is noticed in 17 that the higher magnitude stars are sometimes difficult to pick out from the noise and night airglow. The effect of monitor contrast on the pictures is also evident from the appearance of some stars in figure 1 through 4 (2 sec. integration low monitor contrast) which are not shown in figure 13 (16 sec. integration high monitor contrast), although the beam setting was probably

also different in these two cases. Also compare figures 31 and 32 where both are 2 second integrations but 32 is made with a lower monitor contrast.

The effect of integration times on sensitivity is somewhat hidden in the series of figures 8 to 14 because of the high monitor contrast used. However, figures 35 to 38 were made with a low contrast setting on the monitor and cover the complete range of integration times from 2 to 16 seconds. Here one sees some anomalous behavior which may be a function of the severe shading to be discussed below. This series (35-38) was made with the beam voltage at 92.6 V. For print 35 (2 sec. integration) one sees that the highest camera sensitivity is in the center of the field. However, the successive doubling of the integration times changes the response of the central region very little while the border areas show the expected approach to saturation. Since the night airglow is more or less uniform over the 80^{o} field of figures 35 to 38, one would expect the entire picture from a perfectly operating camera (no shading) to approach uniform brightness as the integration times are increased. This is obviously not the case in figures 35 to 38.

In figures 40 and 41 the beam current was increased by lowering the beam voltage to 92.3 volts. This tends to bring out the bright stars as would be expected. (The opposite is true in figure 46, see section IIA.) Doubling the integration time in 41 over that in 40 shows the same effects observed

in the series 35 to 38. However, in this case the bright central region seems to have expanded somewhat more for the increased integration time than in the corresponding print pair, 35 and 36.

Figure 5 was made with a 0.8 neutral density filter before the I/O camera lens. While the beam voltage was not measured for this exposure it was probably relatively high to compensate for the lower photocathode illumination. The 0.8 neutral density filter reduces the photocathode illumination due to the night sky to a value which approaches that expected for plasma clouds blown off the sun. Figure 5 is thus a record of the camera response to a more or less uniformly bright field (stars excepted) which has a brightness comparable to the weakest light source we hope to detect with the TIGRIS system. The important thing to notice in this picture is the evidence of a high noise level. This is indicated both by the overall horizontal streakiness and the appearance of brighter streaks in the shadow of the building on the horizon. Figure 6 is for 8-sec. integration time with the 0.8 density filter in place. The signal to noise ratio is increased but the use of a higher monitor contrast eliminates most of the night airglow from the picture. It is proposed that large area, low contrast test patterns be used in the calibrated light box to determine the seriousness of this noise at the low light levels.

Figures 18 to 24 show the zodiacal light with Venus in the center of the black spot. The light level is relatively high and the horizon objects are vividly silhouetted against the sky. The black spot spans elongation angles from about 34^{o} to 50^{o}. The total brightness of the sky in this elongation range is about 7×10^{-13} $B_{\odot}$ or 1.3×10^{-4} candles/ft.^{2} ($B_{\odot}$ is the average surface brightness of the solar disk). This results in a photocathode illumination of about 1.3×10^{-5} ft. candles, which is about 2 orders of magnitude greater than that expected for the solar plasma clouds. The long black object in some of the zodical light pictures is a black pole held in front of the I/O camera to contrast with the background sky.

It is perhaps noteworthy as far as sensitivity is concerned that the Andromeda galaxy shows up very clearly just above and to the left of the center of figure 44.

III. LOCALIZED CHANGES IN SENSITIVITY

A. Images of bright stars. In figures 44 and 45 the bright stars appear as grey dots (Notice the bright stars of Cassiopeia and Andromeda in 44 and those of Orion in 45), while higher magnitude stars appear brighter. In print 46 the beam potential was decreased to 91.6 volts and the bright stars in Orion which appeared dim in 45 have now disappeared altogether. This indicates a possible "fatigue" of the photocathode in the image spot of bright stars or secondary

electron effects on the beam side of the target. Figures 8 through 14 which also include Orion were made with the identical beam setting of 92 V as 45 but do not show this effect. The D.C. reference method was different in the two cases, however.

A similarly anomalous behavior of bright star images occurs in figures 1 to 4 where, unfortunately, the beam voltage was not measured. In these prints the bright stars are poorly defined, some being black spots in the centers of bright spread-out rings (α Canis Minor in figure 3) while others are not seen al all (β Canis Minor in figure 3). This is in marked contrast to print 12 where essentially all stars down to 6th magnitude are sharply defined in areas of the field where the camera is most sensitive. However, figures 1 to 4 probably correspond to lower beam currents and again the black centers of stars may be due to secondary electron effects on the beam side of the target.

We have seen above that the images of bright stars can disappear at high beam currents (figure 46). At the same time in figures 18 to 24 the images of the stars ϵ, μ, ζ, γ, η, in Leo disappear at low beam currents. These stars appear as black holes in the bright background of the zodical light. This is probably connected with the occurrence of black centers of some bright stars in figure 3.

B. Long-term desensitization along star trails. An obvious feature of many of the prints is the large number of black streaks which appear whenever the night sky background is discernible. These are identified with the paths of bright stars which pass across the field of view as the earth rotates. In figure 16 the camera is aimed at the celestial equator such that the black streaks are almost straight lines. The stars making the streaks are easily identified in figure 16. The length of the trails in 16 is about 2 hours long, while these same trails are still visible in figure 24 about 1 hour after the camera was pointed in the new direction. This demonstrates the very long time constant for the elimination of these desensitived regions. Another striking example of this desensitization is the trail made by Jupiter in figures 30 to 41. This trail is evident in figure 43 where the camera orientation has been changed.

The existence of these long term paths of desensitization shows that there is a real danger in exposing the photocathode to an extended bright source during the rocket flight. For example, if the image of the bright horizon were accidentally placed on the photocathode during a rocket flight, the system would be completely desensitized for the duration of the flight.

C. Large area of desensitization about bright images of planets. The most obvious feature in figures 18 to 24 and 30 to 41 is the large area of desensitization around the images of the

planets Venus and Jupiter. This is obviously due to the fact that Venus and Jupiter were very bright at the time of the observations, the magnitudes of Venus and Jupiter being about -3.7 and -2.2 respectively. Unlike the star trails, however, this large area desensitization was very transient as evidenced by the fact that tube sensitivity was immediately restored in a black area when the optical field was changed. Only the narrow black trail remained in the new field of view (Compare 42 and 43, which were made only 5 minutes apart).

In 18 to 24, Venus is visible as a faint white spot just below the center of the black area. The first magnitude star, Regulus, appears near the top of the black area as a white spot similar to that of Venus. Regulus is contributing to the densensitization as the black area is elongated along a line between Venus and Regulus. The smeared images near the bottom of the black spot are the stars P, 44, 45, 0 Σ 220 in Leo. There is no object below sixth magnitude which corresponds to the bright doughnut on the right edge of the black area. However, this anomalous bright spot is somehow associated with the effect of Venus and Regulus as it occupies a constant position in the sky.

In figures 30 to 41 Jupiter is visible in the center of the black area. Although this series of pictures was taken with a variety of beam voltages and integration times, there is little or no variation in the size or character of the black area around Jupiter throughout the series. This

indicates that the desensitization of the I/O camera around a bright object may be due entirely to the properties of the photocathode.

Also obvious in prints 30 to 41 is the bright doughnut at the edge of the black area around Jupiter. Like the similar doughnut which was associated with Venus in figures 18 to 24, this bright ring near Jupiter occupies a fixed position in the sky where no significant real object is located. As the bright doughnuts in the two cases occupy different positions with respect to the planet and the trace direction, both electronic and optical explanations of the phenomenon are elusive.

IV. SHADING

Throughout the field test a very severe shading was evident in the camera response. This shading is seen in all pictures made during the tests, but the pattern is best shown in figure 16 which was somewhat overexposed photographically. Figure 16 shows that the shading is a two dimensional function of position which is not linear in either coordinate. The shading was also evident on the oscilloscope as a characteristic time variation in the trace as a picture was scanned. It is noticed in figure 5, for example, that the shading was much less severe than in 16. It is recalled that figure 5 was made through a 0.8 neutral density filter and therefore with a high beam voltage. Figure 16 on the other hand was made with the beam at 92 volts which is

relatively low. This indicates that the severity of shading may be an increasing function of beam current. However, when the pictures of the zodiacal light were made (18-24), an attempt was made to eliminate the shading effect by taking some pictures with the camera rotated by about 90^{o} (19, 21, 22). Even though the beam was set at the high value of 93 V, comparison of 19, 21, 22 with 18, 20, 24 shows that the shading is still too severe to eliminate its effect by camera rotation. As only one image orthicon tube was used throughout the field test is is not known to what extent the severity of the shading is particular to the tube. However, the shading did not appear to be as severe in the lab acceptance test where another I/O tube was used as it did at Capillo Peak.

The variation in shading along the left side of 16 shows that the D.C. reference level was not constant as a function of vertical height. A change in the clamping circuit on the final night of observation did not eliminate this D.C. reference drift although the shading characteristics were changed somewhat. Compare, for example, figure 16 with figure 30, where the latter was made on the last night with the altered clamping circuit. The fact that the D.C. level drift was not eliminated by the change in clamping is indicated in figure 47 where it is seen that the clamping part of the trace is overridden by the drift-causing signal and the trace level is forced below the D.C. reference. Figure 47 shows that the

extent of the drift in level is several times the peak signal. This was not evident in the lab acceptance test and indicates some change in the system characteristics.

In order to get a more quantitative estimate of the shading, oscillograms of single traces across the field of figure 23 were made. Figure 25 is the trace across the upper middle part of figure 23 (i.e. lens open), while figure 26 is the same trace made with the lens capped. The difference between the two traces is the actual light received. The general similarity of the two traces shows that most of the variation in the brightness seen in figure 23 is due to the inherent level shading of the system and not to actual brightness variations in the field of view. Any shading in sensitivity is completely masked by the large variation in level. Figures 27 and 28 are a similar pair of single trace oscillograms, but taken near the bottom of the field. Figure 27 was made with the lens capped while 28 is the same trace with the lens open. The difference between the two traces is now very marked as dark objects are intersected on the horizon. However, the level shading is still evident in the trace of figure 27.

V. DEPENDENCE OF CAMERA CHARACTERISTICS ON ORIENTATION

It is mentioned in section III that an attempt was made to eliminate the camera shading effect by taking two pictures of the same visual field, one with the traces parallel to the

horizon; the other with the traces perpendicular to the horizon. However, when the camera was rotated 90° after the first picture had been made, a marked change in the camera characteristics occurred which was apparently a shift in the D.C. reference of the beam. Adjustment of the monitor brightness and contrast alone seemed to restore the brightness of the second image to that of the first. This may indicate that the camera is not sufficiently magnetically shielded. This dependence of characteristics on orientation must be eliminated before the camera can satisfactorily perform the planned stepped changes in orientation at rocket altitudes.

VI. WHITE EDGE EFFECTS

A white edge is evident along the desensitized track of a star in the upper right hand side of figure 21. In this case the white edge is along the leading side of the black track with respect to the trace. However, this white edge did not appear in figures 19 and 22 which were made under identical camera settings and orientations. A much more pronounced and reproducible white edge appears on the trailing edge of the black pole in figure 29. Comparison of figure 29 with 30, which is the same field of view as 29, shows that the white edge occurs in a region where the camera is much less sensitive because of the shading effect.

VII. STAR IMAGE ERASURE

When the beam current is set to the very low values necessary just to discharge the very faint source highlights, the star images will not be discharged and will therefore appear for several subsequent scans even though the field of view has been changed or the lens capped. If the star images of a given field are not completley erased before changing the camera orientation they will appear in the new field of view along with the new stars and confuse the identication of the new star field. This star field identication may be necessary to determine the direction in which the camera is pointing in the proposed rocket application. In any case, the star fields will be a precise check on any other pointing control which may be used. It is therefore desirable that the target be cleaned up before each change of the field ov view.

The obvious means of cleaning the target of all unwanted images in a short time is to turn the beam current to a high value for several scans while no light is allowed to enter the camera. The test procedure is then to put the camera through the 2-4-8-16 second sequence of integration times with the beam current relatively low. Then the lens of the camera is capped and the beam current simultaneously increased to a predetermined value. The number of scans to erase any evidence of star images on the oscilloscope is then counted. The

oscilloscope was chosen in place of the monitor in order to eliminate the influence of the long persistence tube of the monitor.

A beam voltage of 92 volts was used during the integration time sequence throughout this test, while 92, 91 and 90 volts were used during the erasing scans. The 92 volt value later turned out to be too low for the integration time sequence as a beam voltage near 93 volts just discharged the night airglow image. However, this may not be too serious as the large number of scans necessary to erase the stars with a 92 volt beam indicates that the star images were probably nearly saturated anyway. That is, very little more charge could have accumulated at the position of a given star image if a lower beam current (higher beam voltage) were used for the read out sequence before erasure.

The following table gives the results of the erasure tests.

TABLE I

Beam Volgage	No. Scans for Erasure (lens capped)	Time
92V	30	60-sec.
91V	8	16-sec.
90V	6	12-sec.

Table I indicates that a minimum time of about 10-sec. may be necessary for effective erasure. This length of time can be easily accommodated in the presently proposed time program

for the rocket flight. A higher beam current may reduce this time somewhat, but the time required for erasure seems to level out as the beam voltage is reduced further.

VIII. EFFECT OF LONG PERSISTENCE MONITOR TUBE

In figure 6 the stars have white tails along their circles of rotation about the celestial pole. This is not due to any residual charge effects in the I/O tube but to the fact that bright images on the monitor screen persisted for several minutes after the scan which made them. Hence, the white tails are made up of a series of residual images on the monitor screen. These tails were not present on other prints which were made with the monitor brightness at a lower level. However, it is recommended that all future photographs be taken with a short persistence monitor tube.

IX. SUMMARY

Some of the phenomena described above will probably not hinder the performance of the camera as far as detecting and defining the shapes of faint, extended light sources are concerned, as the camera sensitivity seems perfectly adequate for such detection. The appearance of bright stars as black holes in the otherwise bright background of an extended source may even aid in identifying the direction in which the camera is pointed when at rocket altitudes, since the star field will be otherwise completely washed out. On the other hand,

at least two and perhaps three of the phenomena cannot be tolerated at all, as they make the output of the system very confusing if not entirely meaningless. These are the severe inherent shadings observed in the system, the apparent change in the D.C. reference of the beam with camera orientation and the difficulty of maintaining a constant D.C. reference for a complete scan. These difficulties may be closely related and hence a simultaneous solution may be available.

It may be necessary to subtract electronically the signals from two scans, one made with the lens open the other with the lens closed by a shutter, to obtain an unshaded record of the optical field. If the shading proves to be invariant as a function of beam current the closed lens scan at the beam current to be used could be recorded before any rocket flight and then subtracted on the ground from the telemetered signal of each scan. In fact an average of many closed lens scans could be used to eliminate as much random noise as possible. However too great a reliance on such a subtraction system is not considered sound practice. Furthermore, this method will not eliminate the shading in sensitivity as distinct from the shading in level.

The causes of many of the things observed in the pictures may already be well understood by the television tube experts, and study and consultations are clearly indicated. Those questions which cannot be answered immediately might well be

the specific subject of a further research program. The problems of shading and D.C. reference drift must be resolved before a flight model of the camera can be designed.

T. Gold

T. Gold, Director, CRSR

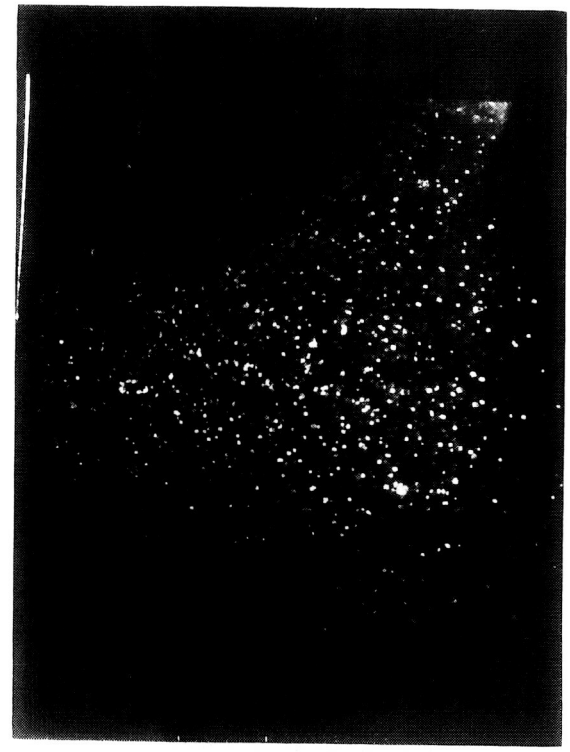

Fig. 2, Canis Minor, 2 sec., 2:35 A.M.

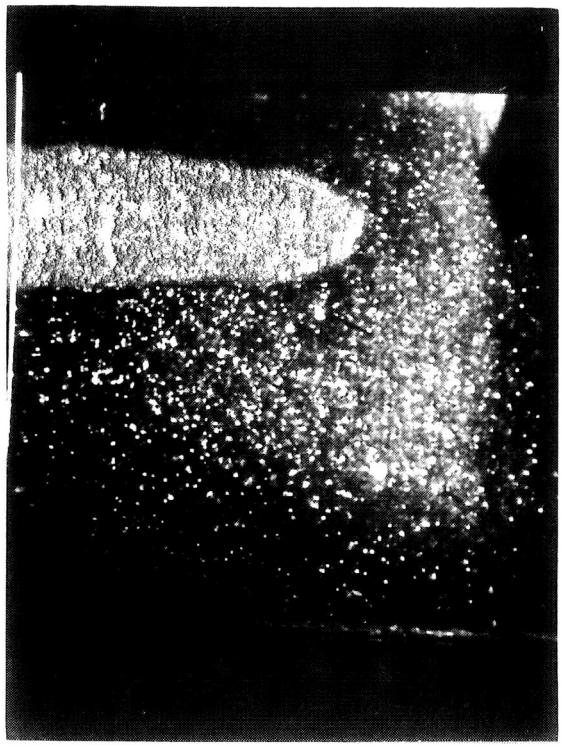

Fig. 4, Canis Minor, 2 Sec., 2:45 A.M.

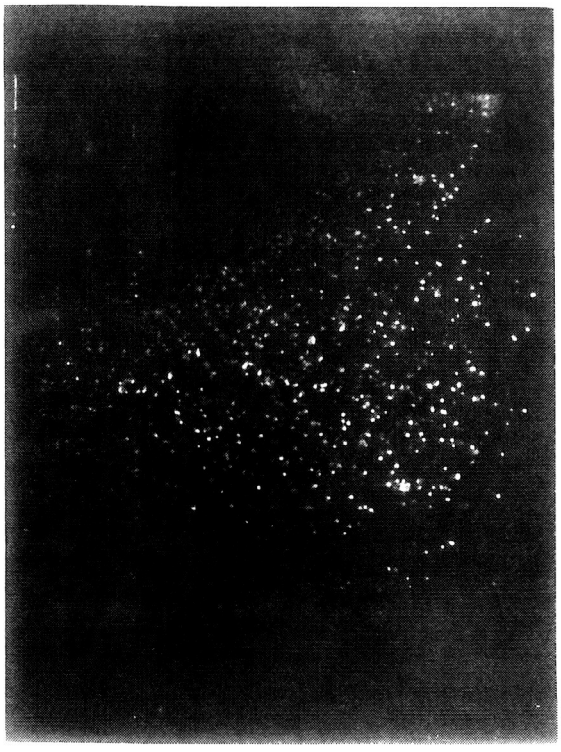

Fig. 1, Canis Minor, 2 sec., 2:30 A.M.

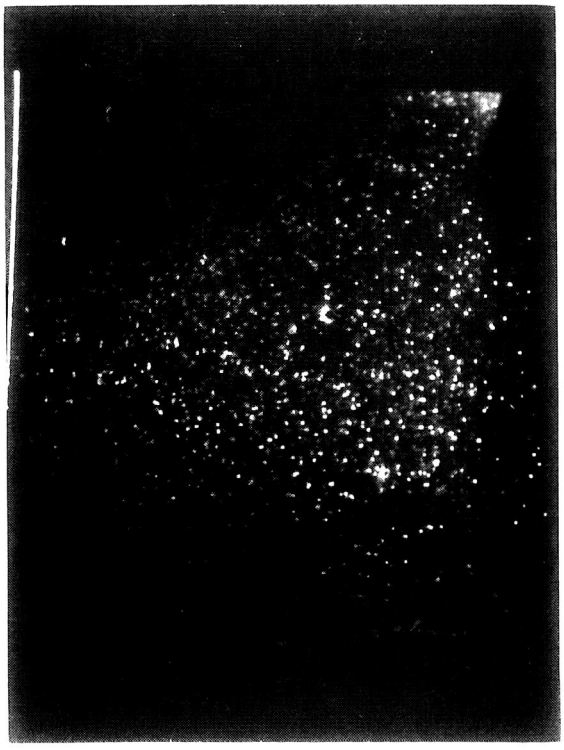

Fig. 3, Canis Minor, 2 Sec., 2:40 A.M.

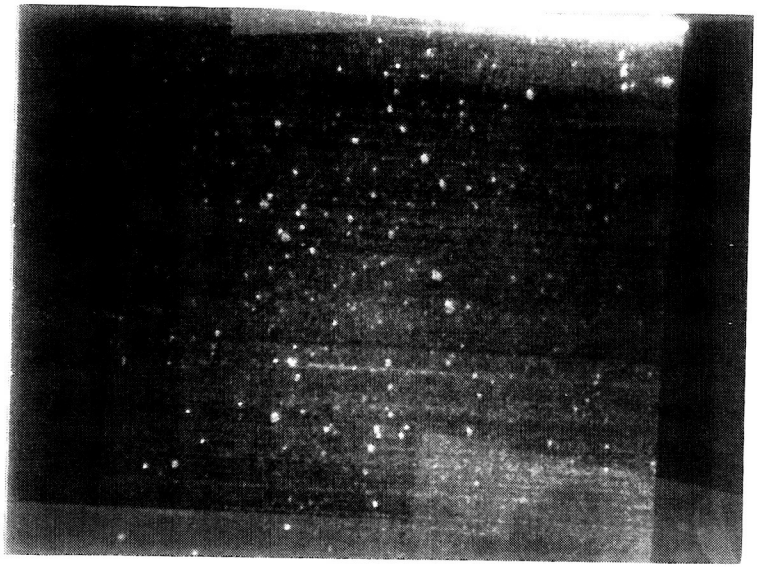

Fig. 5, Canis Minor, 2 Sec., 0.8 ND filter, 3:00 A.M.

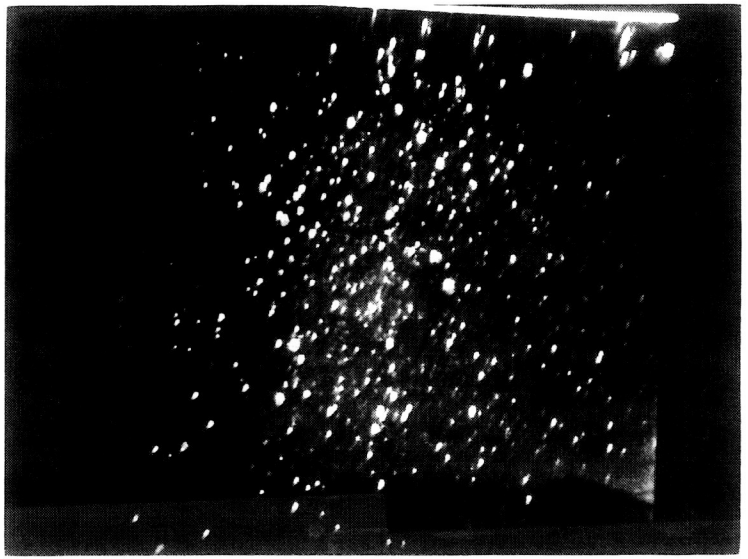

Fig. 6, Canis Minor, 8 Sec., 0.8 ND filter, 3:10 A.M.

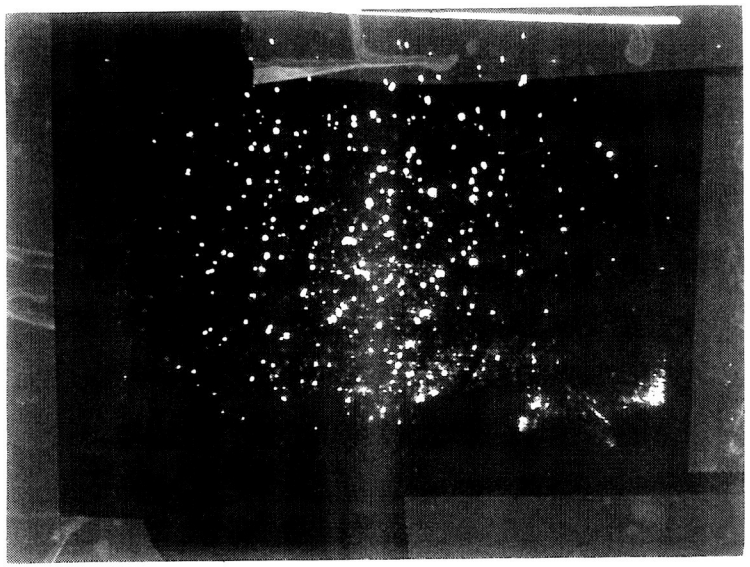

Fig. 7, Ursa Major, 8 Sec., 0.8 ND filter, 4:50 A.M.

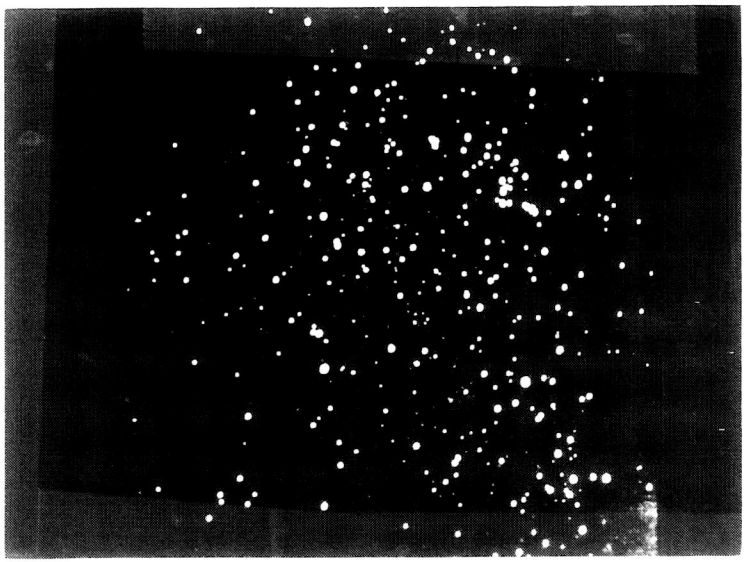

Fig. 8, Canis Minor, Orion, 2 Sec., 92.0 V, 2:55 A.M.

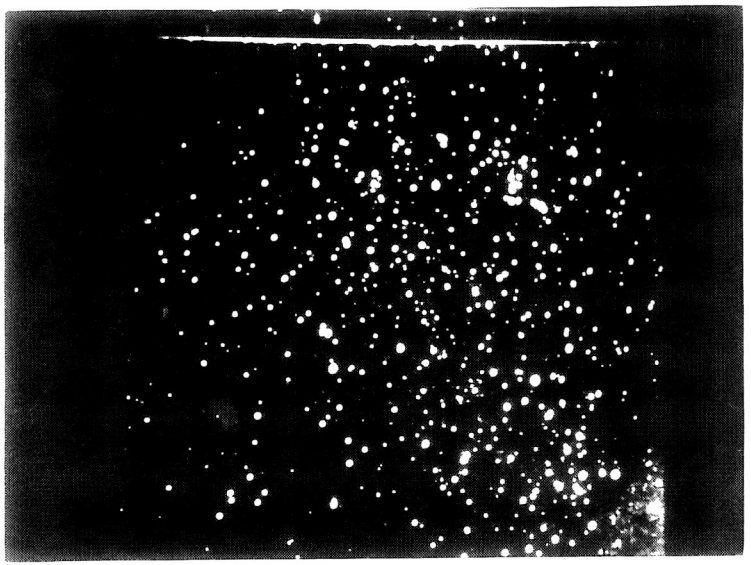

Fig. 9, Canis Minor, Orion, 4 Sec., 92.0 V,
2:58 A.M.

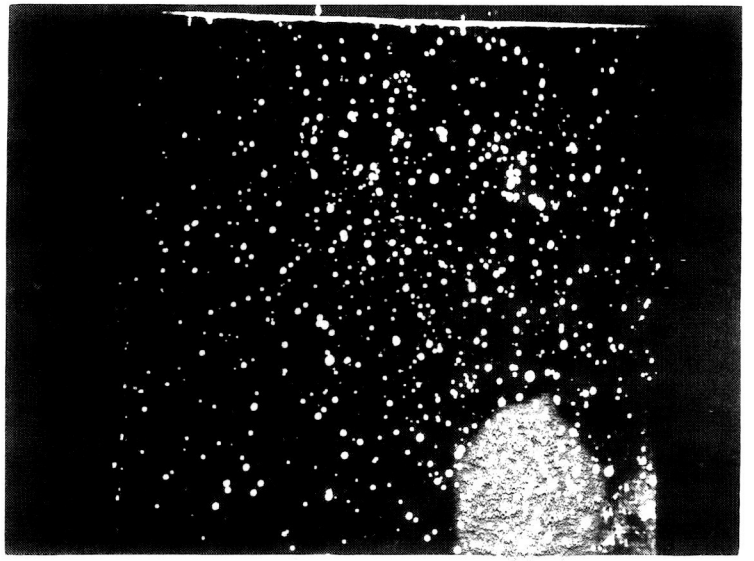

Fig. 10, Canis Minor, Orion, 6 Sec., 92.0 V
3:00 A.M.

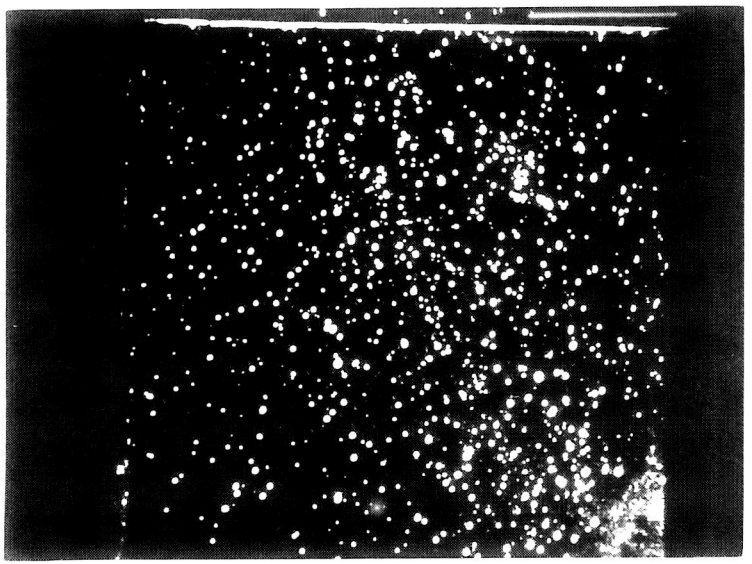

Fig. 11, Canis Minor, Orion, 8 Sec., 92.0 V,
3:01 A.M.

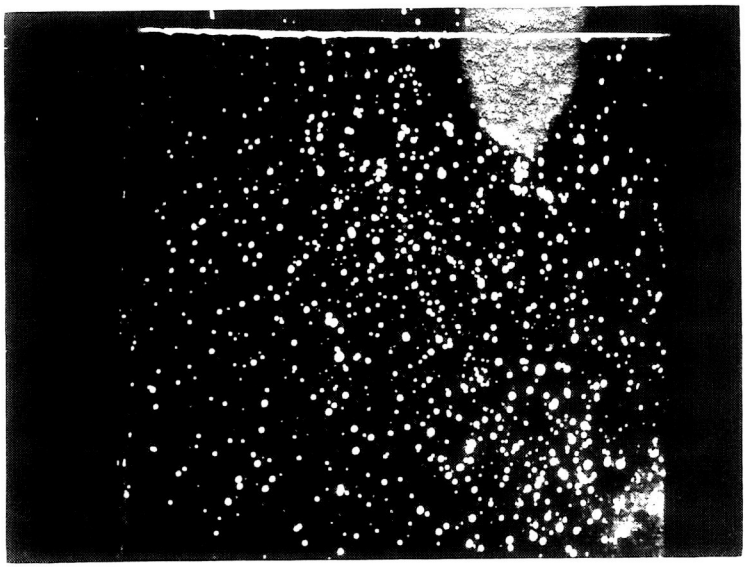

Fig. 12, Canis Minor, Orion, 10 Sec., 92.0 V,
3:05 A.M.

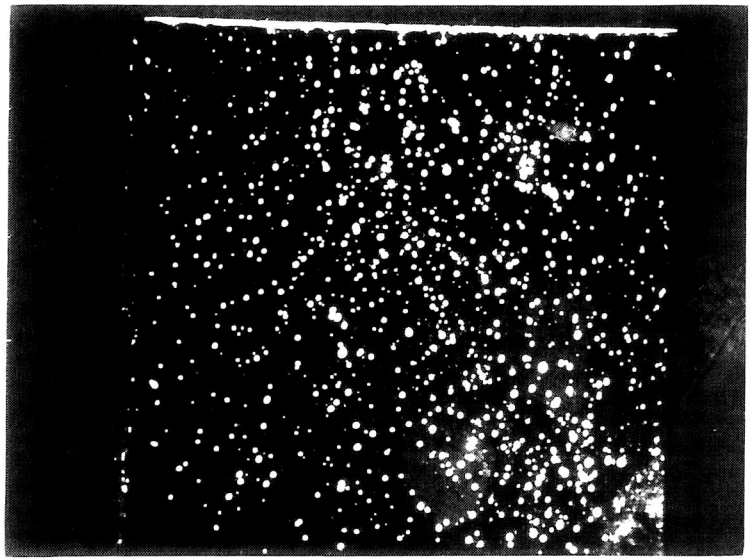

Fig. 13, Canis Minor, Orion, 16 Sec., 92.0 V. 3:06 A.M.

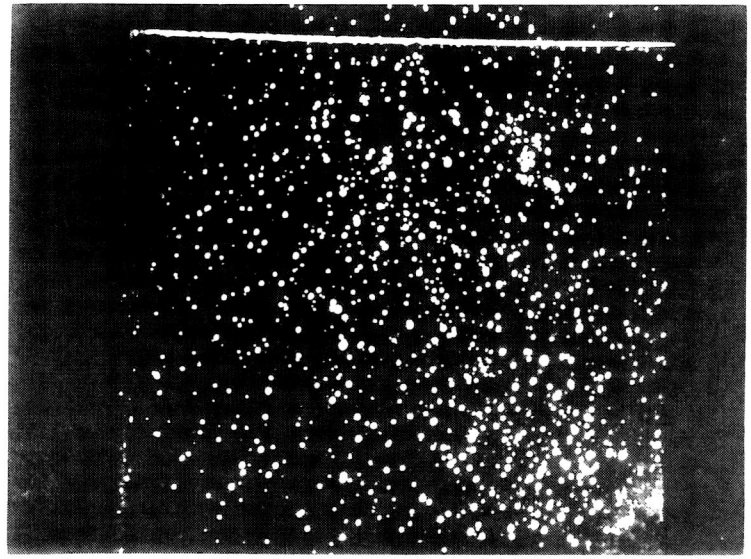

Fig. 14, Canis Minor, Orion, 32 Sec., 92.0 V, 3:07 A.M.

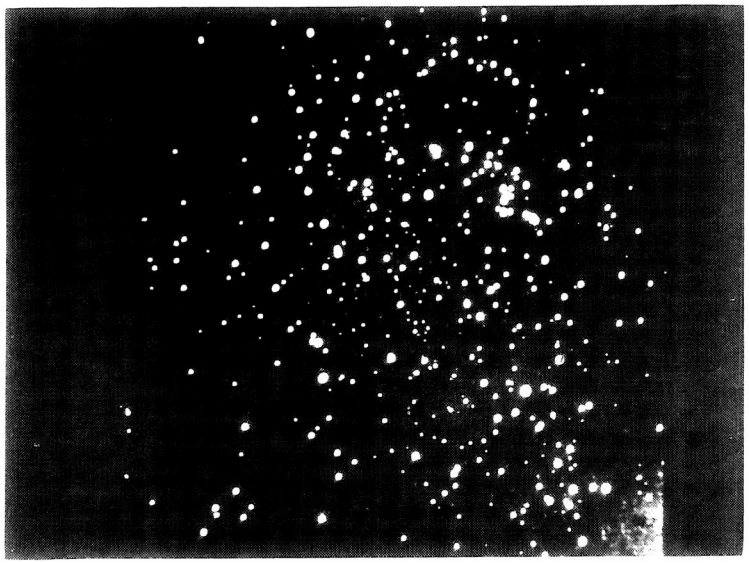

Fig. 15, Canis Minor, Orion, 2 Sec., 92.0 V, 3:10 A.M.

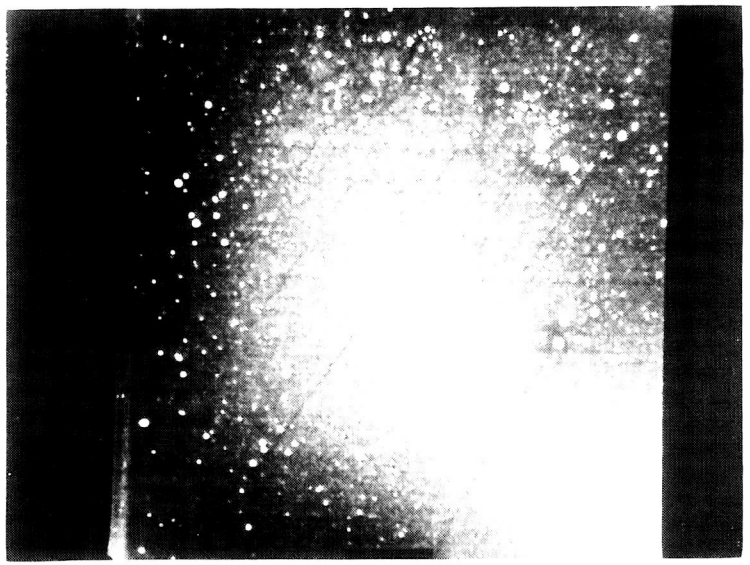

Fig. 16, Canis Minor, Orion, 2 Sec., 92.0 V, 3:15 A.M.

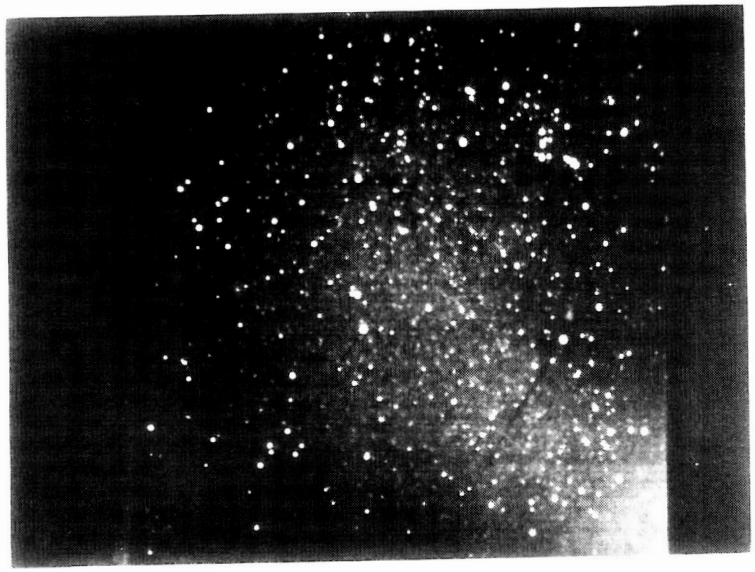

Fig. 17, Canis Minor, Orion, 2 Sec., 92.0 V, 3:20 A.M.

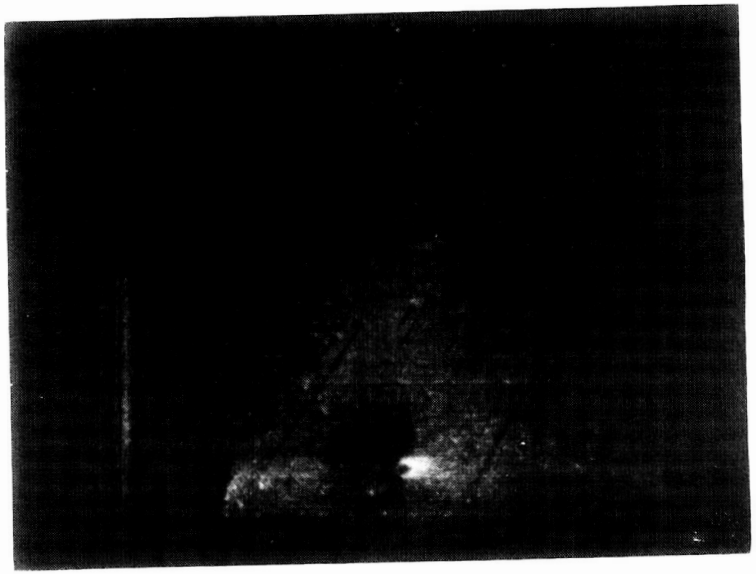

Fig. 18, Leo, Venus, Zodiacal Light, 2 Sec., 93.0 V, 3:35 A.M.

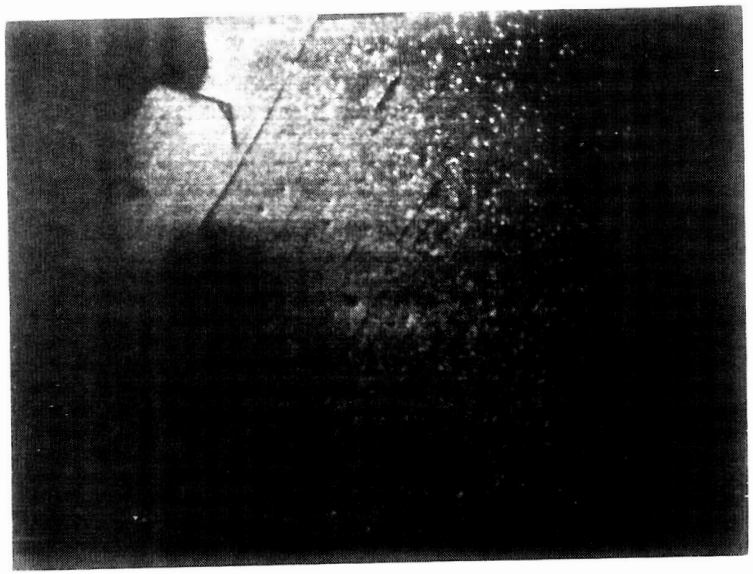

Fig. 19, Leo, Venus, Zodiacal Light, 2 Sec., 93.0 V, 3:50 A.M.

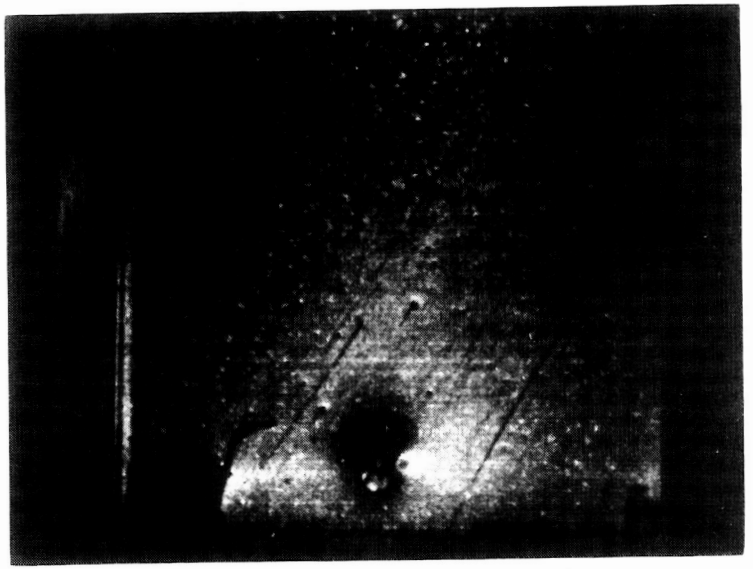

Fig. 20, Leo, Venus, Zodiacal Light, 2 Sec., 93.0 V, 3:53 A.M.

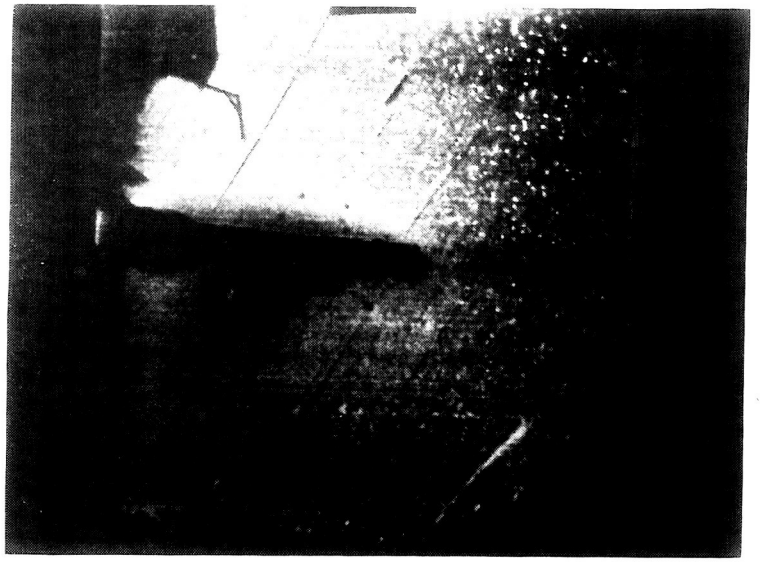

Fig. 21, Leo, Venus, Zodiacal Light, 2 Sec., 93.0 V, 3:59 A.M.

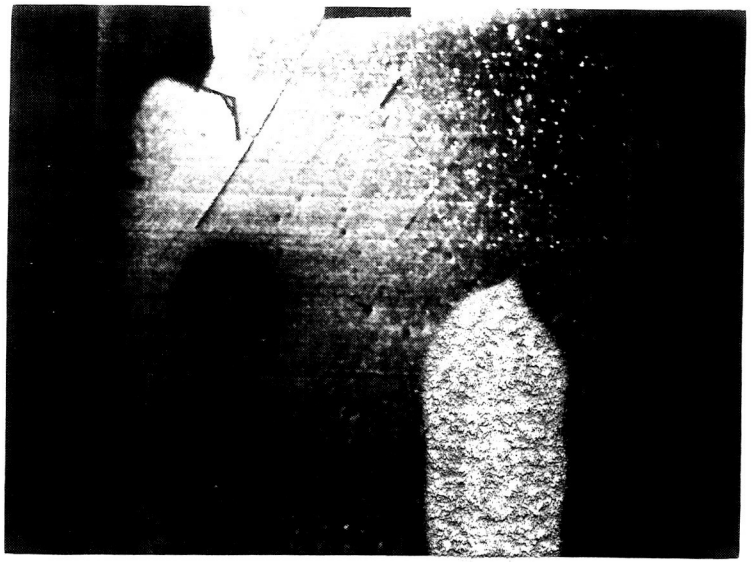

Fig. 22, Leo, Venus, Zodiacal Light, 2 Sec., 93.0 V, 4:00 A.M.

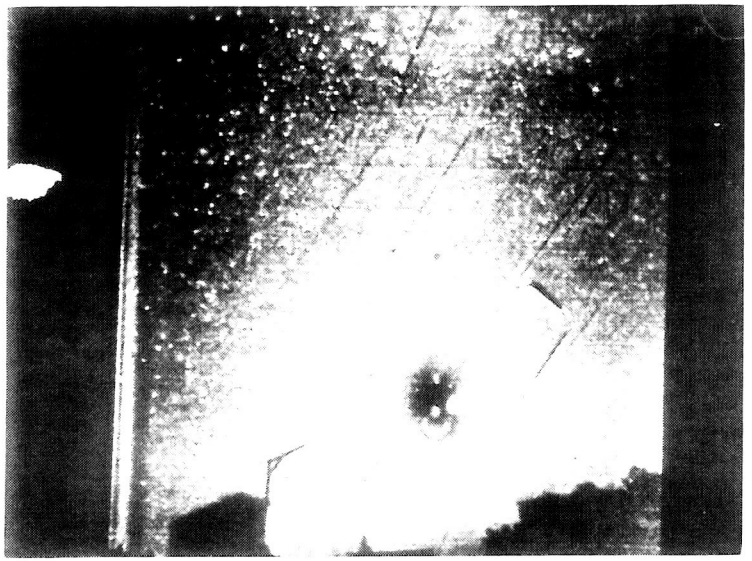

Fig. 23, Leo, Venus, Zodiacal Light, 2 Sec., 93.0 V, 4:05 A.M.

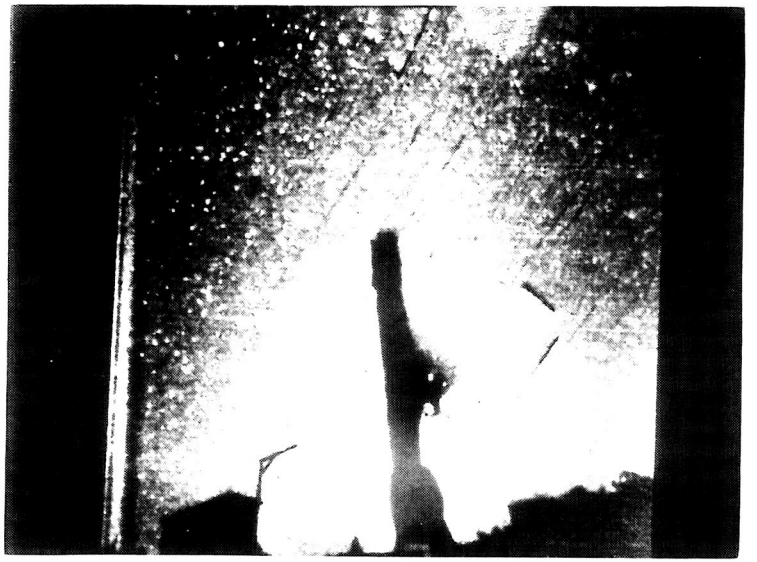

Fig. 24, Leo, Venus, Zodiacal Light, 2 Sec., 93.0 V, 4:07 A.M.

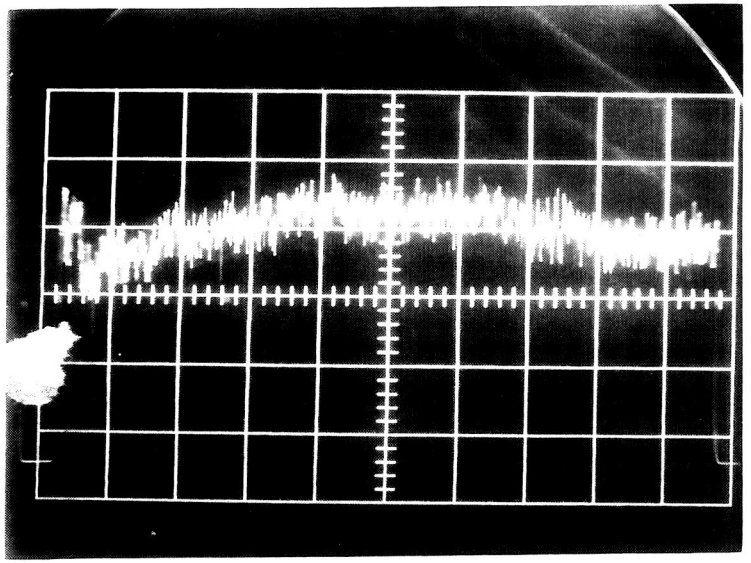

Fig. 25, Oscillogram of single trace just above middle of Fig. 23.

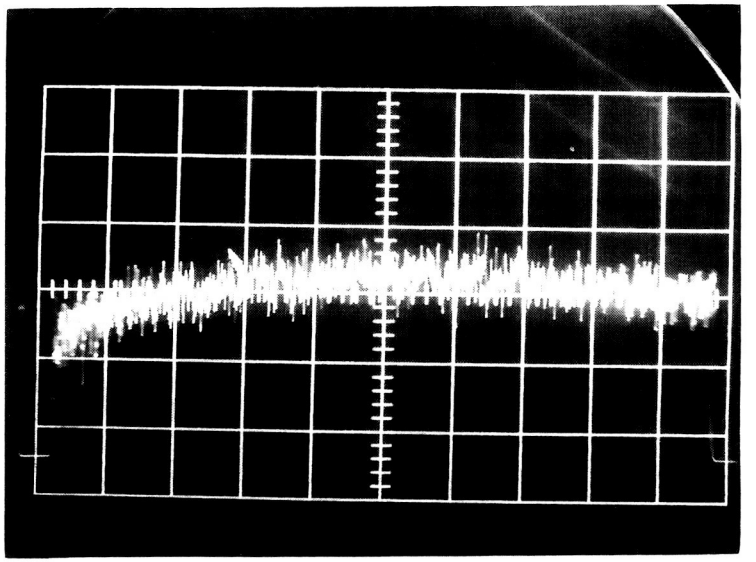

Fig. 26, Oscillogram of same trace as in Fig. 25 but with lens capped.

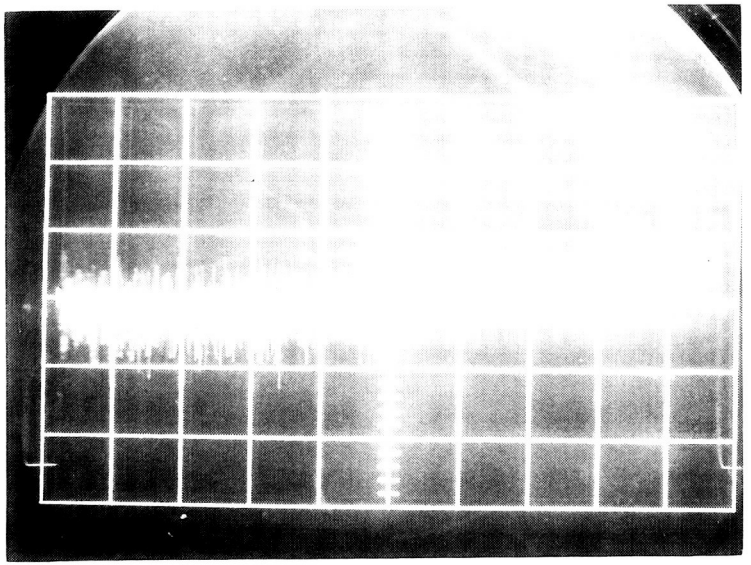

Fig. 27, Oscillogram of trace near bottom of frame with lens capped.

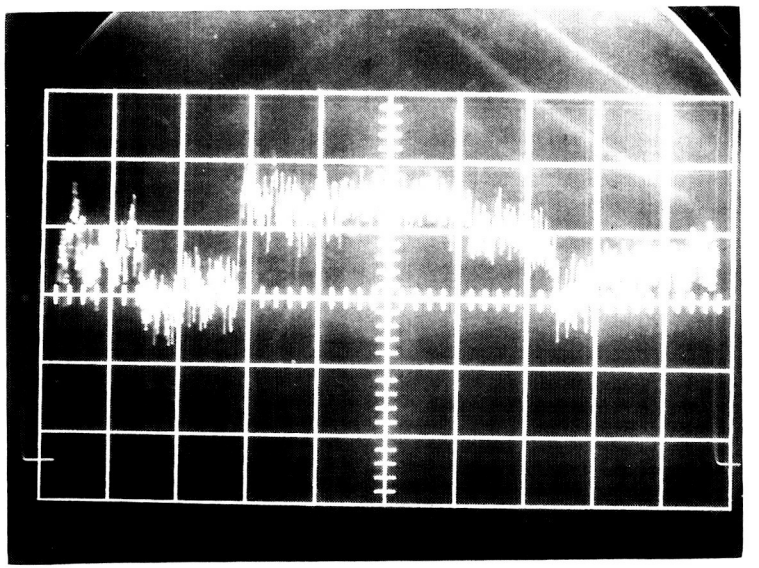

Fig. 28, Oscillogram of same trace as in Fig. 27 but with lens open to field of Fig. 23.

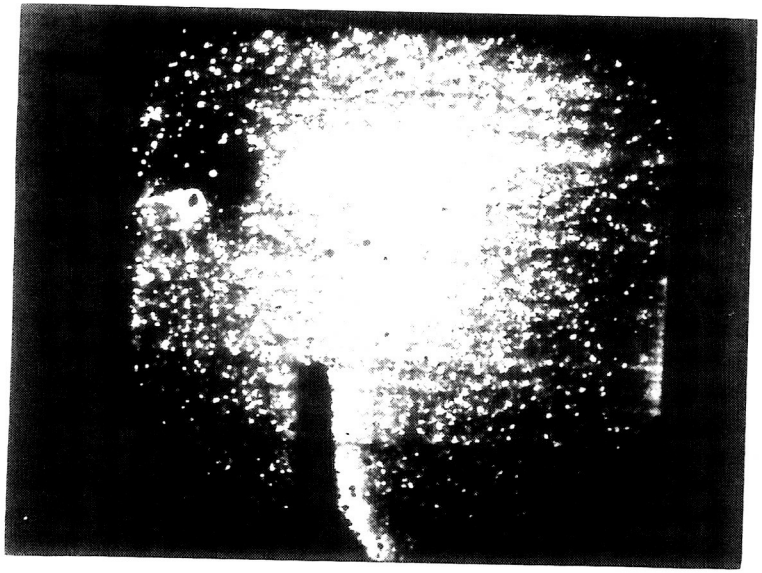

Fig. 29, Eridanus, Taurus, Jupiter, 2 Sec., 92.9 V, 12:55 A.M.

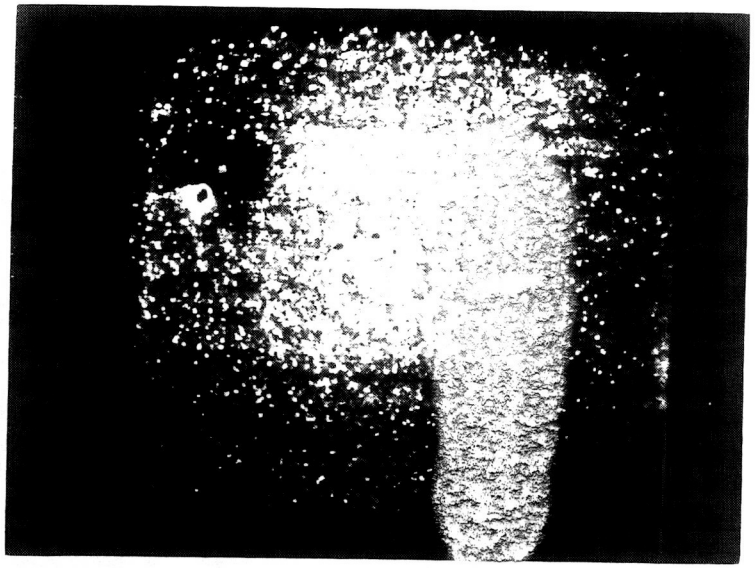

Fig. 30, Eridanus, Taurus, Jupiter, 2 Sec., 92.9 V, 12:5[illegible] A.M.

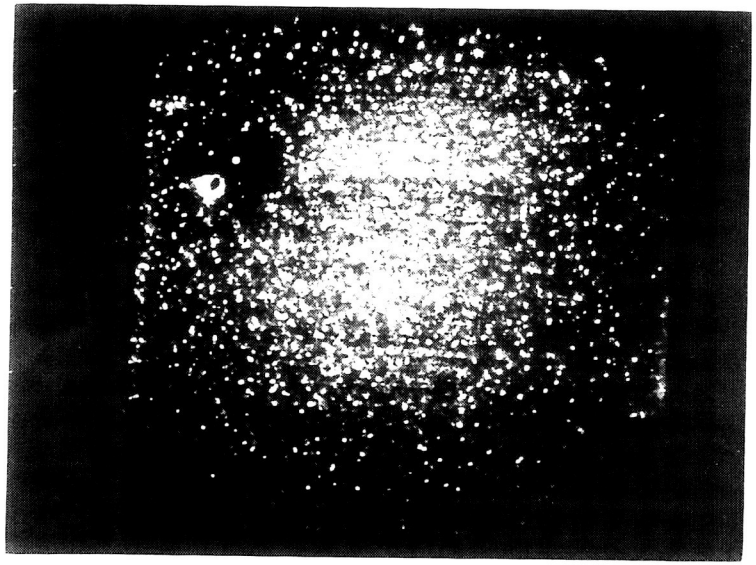

Fig. 31, Eridanus, Taurus, Jupiter, 2 Sec., 92.8 V, 1:00 A.M.

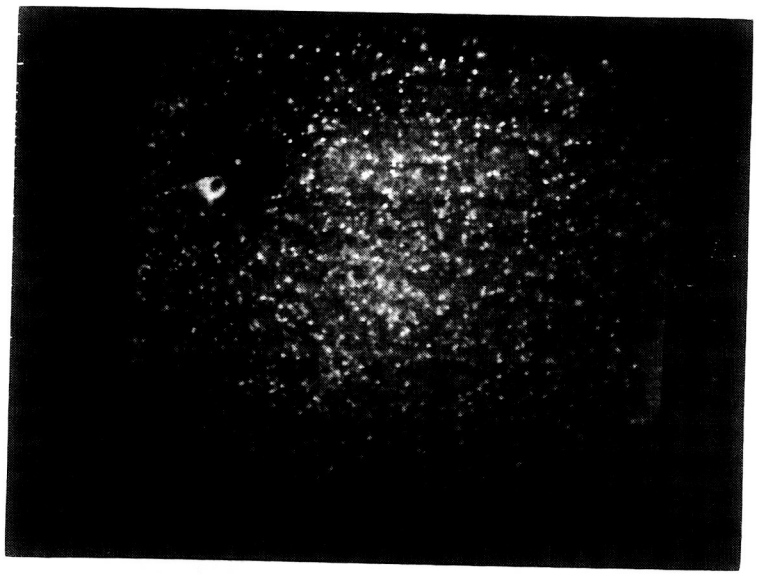

Fig. 32, Eridanus, Taurus, Jupiter, 2 Sec., 92.8 V, 1:05 A.M.

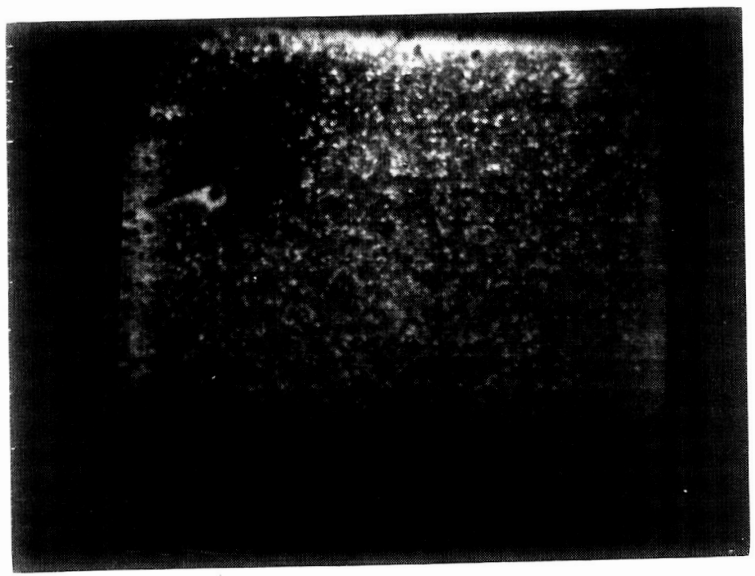

Fig. 33, Eridanus, Taurus, Jupiter, 4 Sec., 92.8 V, 1:06 A.M.

Fig. 34, Eridanus, Taurus, Jupiter, 2 Sec., 92.8 V, 1:15 A.M.

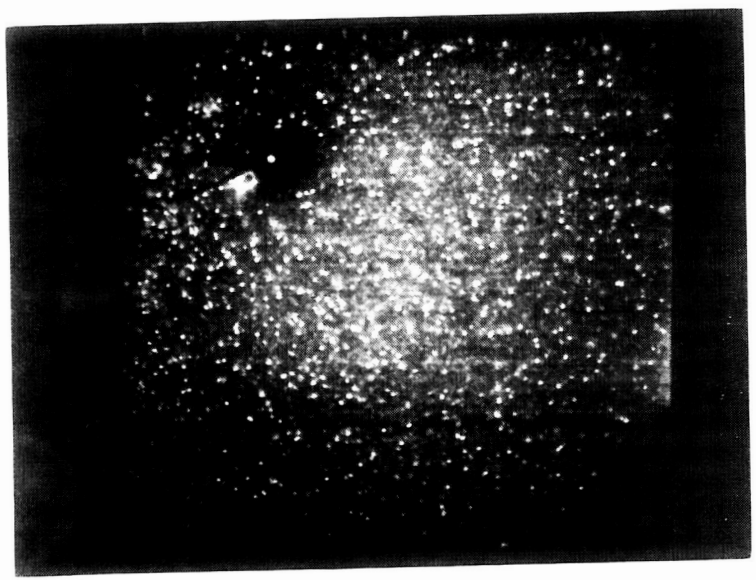

Fig. 35, Eridanus, Taurus, Jupiter, 2 Sec., 92.6 V, 1:20 A.M.

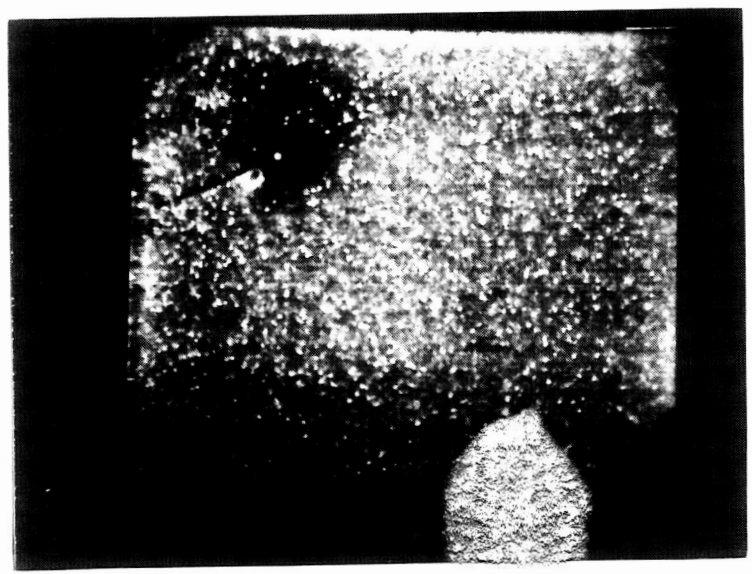

Fig. 36, Eridanus, Taurus, Jupiter, 4 Sec., 92.6 V, 1:22 A.M.

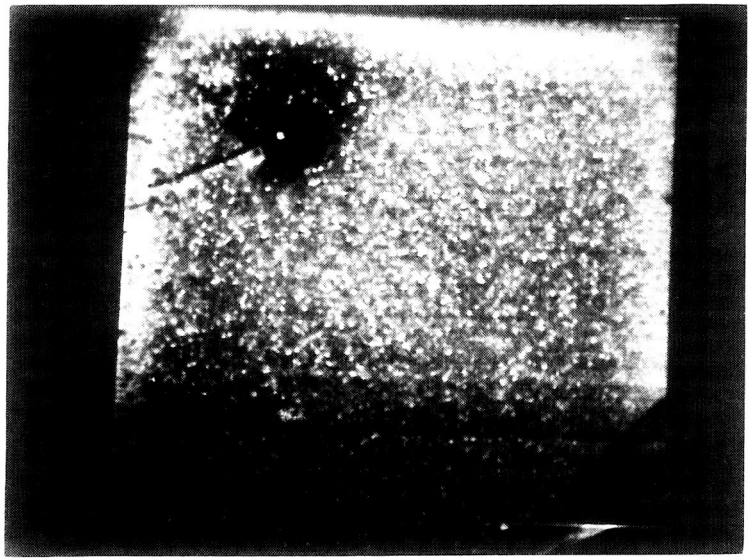

Fig. 37, Eridanus, Taurus, Jupiter, 8 Sec., 92.6 V, 1:25 A.M.

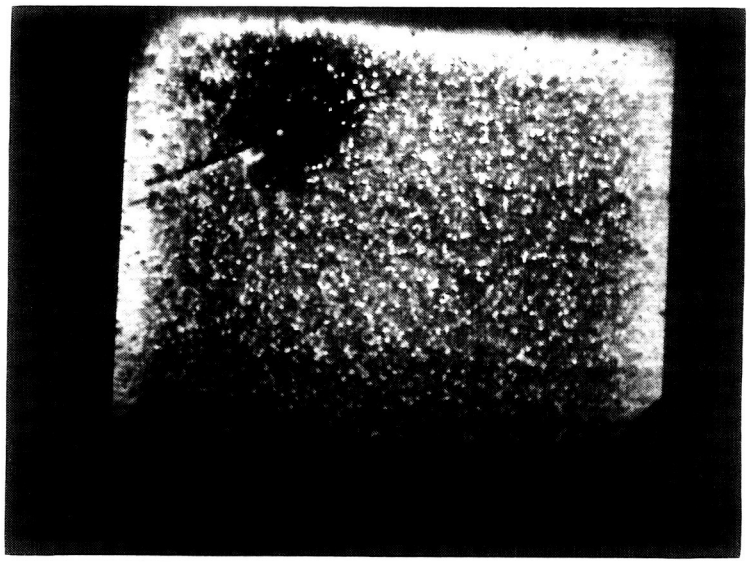

Fig. 38, Eridanus, Taurus, Jupiter, 16 Sec., 92.6 V, 1:27 A.M.

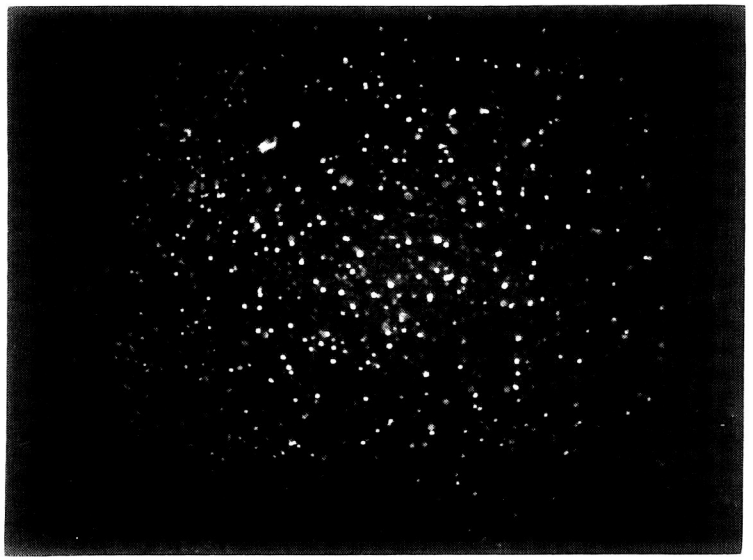

Fig. 39, Eridanus, Taurus, Jupiter, 2 Sec., 92.3 V, 1:35 A.M.

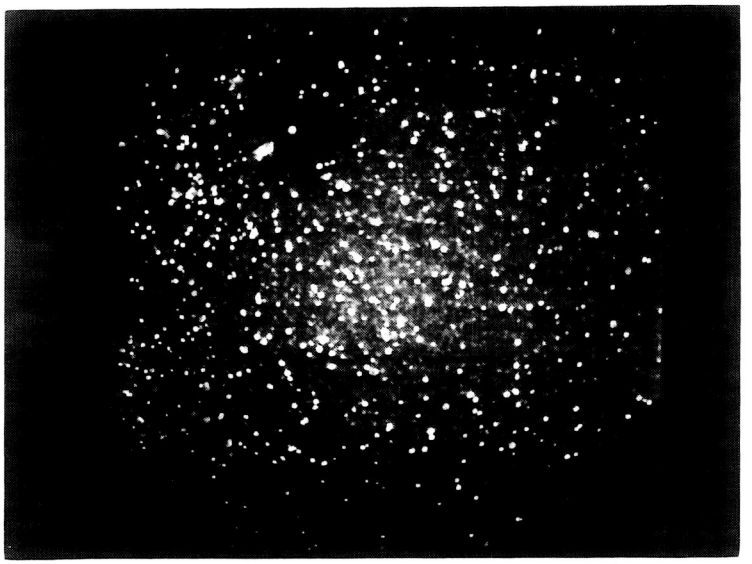

Fig. 40, Eridanus, Taurus, Jupiter, 2 Sec., 92.3 V, 1:36 A.M.

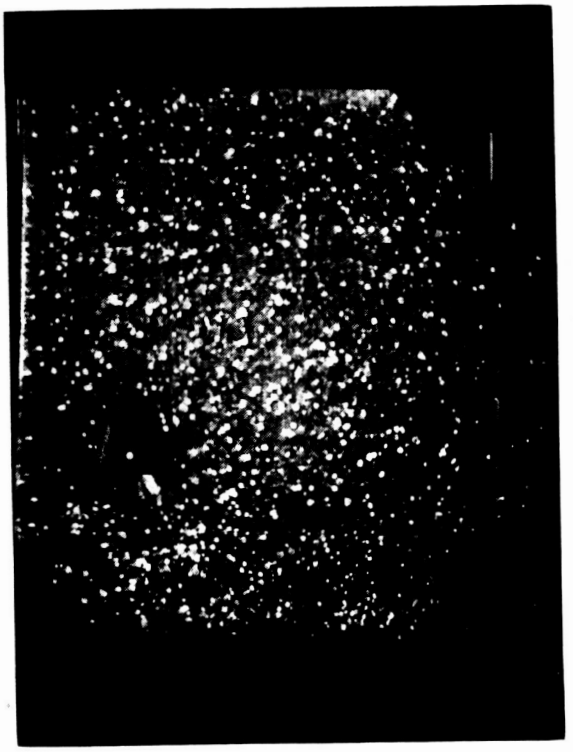

Fig. 41, Eridanus, Taurus, Jupiter, 4 Sec., 92.3 V, 1:40 A.M.

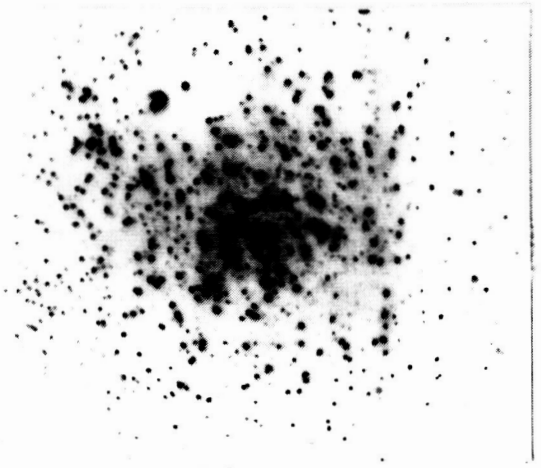

Fig. 42, Jupiter, Taurus, Eridanus, 2 sec, 92.3V, 2:00 A. M.

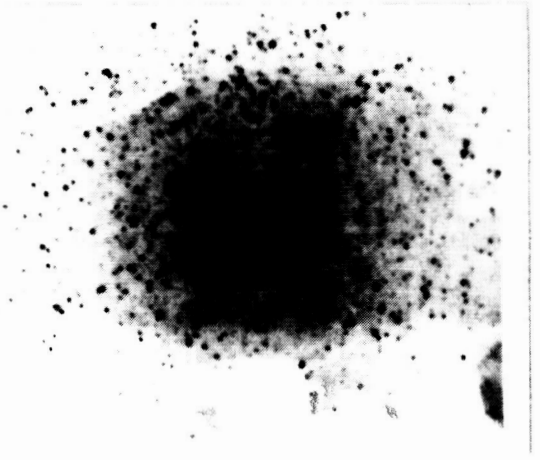

Fig. 43, Ursa Major, 2 sec., 92.3V 2:05 A. M.

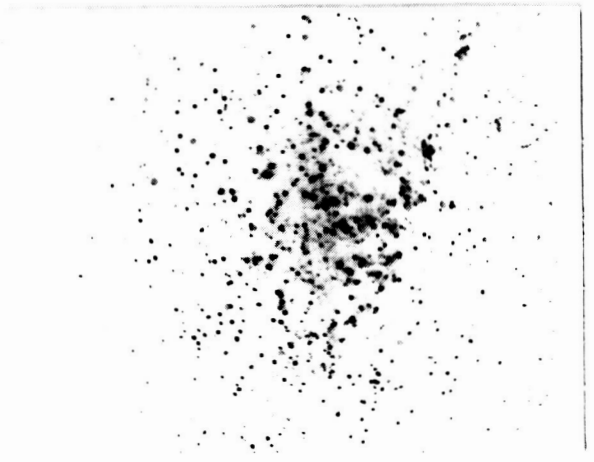

Fig. 44, Andromeda, Cassiopeia, 2 sec., 92.3V, 2:15 A. M.

Fig. 45, Orion, 2 sec., 92.0V, 2:38 A. M.

Fig. 46, Orion, 2 sec., 91.6V 2:40 A. M.

Fig. 47, Range of trace level for one scan.